BUTTERWORTH HEINEMANN

Numerical analysis of the thermal convection for Herschel–Bulkley fluids

C. Nouar, M. Lebouché, and R. Devienne
Laboratoire d'Energétique et de Mécanique Théorique et Appliquée, Vandoeuvre-les-Nancy, France

C. Riou
EDF, Direction des Etudes et Recherches, Département Transfert Thermique et Aérodynamique, Chatou, France

This article presents a numerical analysis of the laminar forced convection in a cylindrical duct for a thermodependent Herschel–Bulkley fluid. Two boundary conditions are considered: constant wall heat flux and constant wall temperature. Both fluid flow and heat transfer are studied. The governing equations are solved using the finite difference method with an implicit scheme. It is assumed that all fluid properties other than consistency K, are constant. The K–T relation used is $K = K_0 \exp(-bT)$. The results obtained enable us to characterize completely the dynamic and thermal fields structure. For a practical use of the computed results, correlations for local Nusselt number and pressure gradient are proposed taking into account the modification of the wall shear rate induced by the rheological properties and the temperature-dependent character of the fluid.

Keywords: Herschel–Bulkley fluids; cylindrical duct; heat transfer; pressure drop

Introduction

In industries such as food, chemical, polymer, and petrochemical processing, non-Newtonian fluids are subjected to some thermal processing. Generally, the physical properties of these fluids are very sensitive to temperature. This has some effects on the velocity profile and the radial temperature profile, and therefore, on the pressure drop and the heat transfer rate. The case of Ostwald fluids, thermodependent by their consistency K, has been dealt with in many publications. However, few studies have been dedicated to the yield stress fluids, although they are frequently encountered in food and chemical industries. The present article intends to contribute to the study of the thermal convection in a pipe for a fluid whose rheological behavior can be described by the Herschel–Bulkley law: $\tau = \tau_s + K|\dot{\gamma}|^n$. Bird et al. (1983) have given a list of some materials that fall into this category of fluids (e.g., coal/Newtonian liquid, applesauce, etc.). All the physical properties of the fluid are assumed to be constant, except for the consistency K. Two boundary conditions have been considered: constant wall temperature and constant wall heat flux. For each of these boundary conditions, the dynamic and thermal fields structure is analyzed, respectively, through the evolution of the velocity profiles and that of the heat transfer coefficient. Correlations are presented that link the pressure gradient and the heat transfer coefficient to the dimensionless numbers relative to the flow, to the heating conditions, and to the rheological properties of the fluid.

Literature review

In the beginning, the theoretical studies dealing with heat transfer for non-Newtonian fluids were based on the assumption of temperature-independent physical properties. Pigford (1955) employed the Lévêque method, which had been successfully applied to nonisothermal flow of Newtonian fluids in cylindrical pipe. Lyche and Bird (1956) and Whiteman and Drake (1958) extended the second Graetz problem to power-law fluids in circular tube, and Hirai (1959) and Wisler and Schester (1959) presented the solution of the Graetz problem for Bingham fluids. Others who have considered the case of the simultaneously developing dynamic and thermal boundary layers are Chandrupatla and Sastri (1978) for a pseudoplastic fluid, Lin and Shah (1978) for a Herschel–Bulkley fluid, and Vradis et al. (1992) for a Bingham plastic fluid. However, most fluids encountered in the food industry have a high Prandtl number, the predictions of heat transfer parameters can be achieved by considering that the flow is established through the entire length of the duct without involving significant error. To take the variation of rheological properties into consideration, especially the consistency K, with temperature, Metzner et al. (1957) suggested, for an Ostwald fluid with a constant wall

Address reprint requests to Dr. C. Nouar, Lemta-Ensem, 2 Avenue de la Foret de Haye, B. P. 160, 54504 Vandoeuvre-Les-Nancy-Cedex, France.

Received 21 September 1994; accepted 19 January 1995

Int. J. Heat and Fluid Flow 16: 223–232, 1995

655 Avenue of the Americas, New York, NY 10010

0142-727X/95/$10.00
SSDI 0142-727X(95)00010-N

temperature heating, an empirical correction factor similar to that used by Sieder and Tate: $Nu = 1.16(\pi/2X^+)^{1/3}\Delta^{1/3}(K_m/K_p)^{0.14}$, for $X^+ < 0.02$. The factor Δ is the ratio of the wall shear rate to the one that would be obtained for a Newtonian fluid at the same flow rate. It represents the modification of the wall shear rate attributable to the rheological properties of the fluid. The correction factor attributable to the variation of the consistency with respect to temperature is $(K_m/K_p)^{0.14}$. Another expression of this factor for the mean Nusselt number, was proposed by Kwant et al. (1973a and 1973b). It is given by $1 + 0.271\ \mathrm{Ln}\ \Phi + 0.023\ (\mathrm{Ln}\ \Phi)^2$ with $\Phi = (1 - \alpha' b(T_p - T_e))^{1/n}(X^+/0.6)^{-\alpha' b(T_p - T_e)}$, where α' is a function of n and $b(T_p - T_e)$. In the case of constant flux heating for an Ostwald fluid, Mizushina et al. (1967) showed that the exponent of K_m/K_p is a function of the power-law index n and proposed a correlation of the form: $Nu = 1.41(\pi/2X^+)^{1/3}\Delta^{1/3}(K_m/K_p)^{0.1/n^{0.7}}$, for $X^+ < 0.05$, and $Nu = 4.36\Delta^{1/3}(K_m/K_p)^{0.14/n^{0.7}}$, for $X^+ \geq 0.05$.

Joshi and Bergles (1980a and 1980b), from a theoretical development and experimental tests, proposed another expression of the consistency ratio power in the thermal entrance region: 0.58–0.44 n. When the thermal regime is developed, the correction factor was given by a second order polynomial in $(b\phi_p D/2\lambda)$, where b characterizes the variation of the consistency with the temperature $K = K_0\exp(-bT)$. From the numerical solution of the conservation equations and based on the test results of Scirocco et al. (1985), Kahine et al. (1993) offered a more useful correction factor, given by $(b\phi_p D/2\lambda)^{0.14/n^{0.7}}$.

In the case of the yield-stress fluids, Forest and Wilkinson (1973) have supplied diagrams giving the evolution of the Nusselt number as a function of the Graetz number with dimensionless groups specifying the temperature dependence effect and the rheological properties and the wall conditions as parameters. The authors gave neither any correlation nor any results concerning the pressure drop. Moreover, the range of the rheological parameters considered is rather limited. Naïmi et al. (1990) have presented the effect of the dimension of the plug core on the corrective factor. They mentioned, experimentally, in the case of an annular geometry, that an increase of the plug core width leads to a decrease of the thermodependency effects. The last point has not been studied from a quantitative point of view. This bibliographic review shows the necessity of a supplementary study for temperature-dependent yield stress fluids, which we have performed numerically.

Basic equations

The fluid is incompressible and thermodependent by its consistency K. The viscous energy dissipation is considered, and the axial diffusion is neglected in comparison with the radial diffusion. At the entrance of the heated region ($z = 0$), the flow is fully developed, and the fluid temperature is constant and uniform. The coordinate system, the axial and radial components of the velocity, are illustrated in Figure 1. The following dimensionless parameters are used:

$$U = \frac{u}{U_d};\quad V = \frac{v}{U_d};\quad Z = \frac{\rho z U_d}{\mu_0},\quad P = \frac{p}{\rho U_d^2};$$

$$\overline{\mu_a} = \frac{\mu_a}{\mu_0};\quad \theta = \frac{TCp}{U_d^2};\quad \bar{\lambda} = \frac{\lambda}{\mu_0 Cp};\quad \eta = \frac{\rho U_d r}{\mu_0};$$

$$\eta_0 = \frac{\rho U_d R}{\mu_0};\quad Y = \frac{\rho U_d y}{\mu_0}$$

where $y = R - r$, and $Y = \eta_0 - \eta$. The apparent viscosity of the fluid calculated at the local temperature T is μ_a, and μ_0 corresponds to the apparent viscosity calculated at the wall shear rate for a fully developed velocity profile and at the inlet temperature T_e.

The problem is governed by the following equations:

Continuity equation:

$$\frac{\partial}{\partial Z}(\eta U) + \frac{\partial}{\partial Y}(\eta V) = 0 \tag{1}$$

Z momentum equation:

$$U\frac{\partial U}{\partial Z} + V\frac{\partial U}{\partial Y} = -\frac{\partial P}{\partial Z} + \frac{1}{\eta}\frac{\partial}{\partial Y}\left[\eta\overline{\mu_a}\frac{\partial U}{\partial Y}\right] \tag{2}$$

Notation

ap	relative radius of the plug core (nonsheared zone) $ap = R_s/R$
b	$K = K_0\exp(-bT)$
Cp	specific heat, $J \cdot kg^{-1} \cdot C^{-1}$
Br	Brinkman number $Br = \mu_0 U_d^2/[\lambda(T_e - T_p)]$
D	diameter of pipe, m
K	fluid consistency, $Pa \cdot s^n$
m	reverse of the power-law index
n	power-law index of the fluid
Nu	local Nusselt number
p	pressure, Pa
P	dimensionless pressure
r	radial coordinate, m
R	radius of pipe, m
R_s	outer radius of the plug core, m
u	axial velocity, m/s
U	dimensionless axial velocity
U_d	average velocity of the flow, m/s
T_e	inlet temperature, C
v	radial velocity, m/s
V	dimensionless radial velocity
X^+	Cameron number $X^+ = 2\lambda z/\rho Cp U_d D^2$
y	radial coordinate $y = R - r$ (m)
z	axial coordinate, m

Greek

Δ^*	wall shear rate compared to that of a Newtonian fluid
η	dimensionless radial position
μ	viscosity, $Pa \cdot s$
ρ	fluid density, $kg \cdot m^{-3}$
τ_s	yield stress, Pa
ϕ_p	wall heat flux density, $W \cdot m^{-2}$

Subscripts

e	inlet
m	bulk
New	Newtonian
p	wall
cp	constant physical properties
vp	variable physical properties

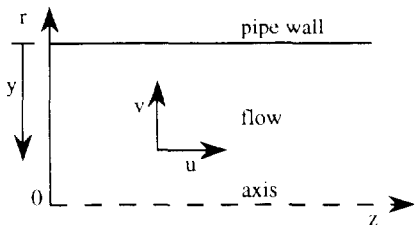

Figure 1 System of coordinates

Energy equation:

$$U\frac{\partial\theta}{\partial Z}+V\frac{\partial\theta}{\partial Y}=\frac{1}{\eta}\frac{\partial}{\partial y}\left[\eta\bar{\lambda}\frac{\partial T}{\partial y}\right]+\overline{\mu_a}\left[\frac{\partial U}{\partial Y}\right]^2 \tag{3}$$

Continuity equation in the integral form:

$$\int_0^{\eta_0}\eta U\,\mathrm{d}\eta=\tfrac{1}{2}\eta_0^2 \tag{4}$$

Rheological behavior:

$$\overline{\mu_a}=\frac{\tau_s}{\rho U_d^2}\left|\frac{\partial U}{\partial Y}\right|^{-1}+\frac{K}{\mu_0}\left[\frac{\rho U_d^2}{\mu_0}\right]^{n-1}\left|\frac{\partial U}{\partial Y}\right|^{n-1};\quad \tau>\tau_s \tag{5a}$$

$$\partial U/\partial Y=0;\quad \tau\le\tau_s \tag{5b}$$

Rheological studies performed by Nouar et al. (1994) and Naïmi et al. (1990) on a model fluid that could represent a large range of liquid foods show that these fluids are thermodependent essentially by their consistency K within a range of temperatures 10–60°C. The relation K–T adopted is $K = K_0 \exp(-bT)$. The temperature dependency of the yield stress τ_s and the power law index n is weak compared with the temperature dependency of the consistency K and, thus, can be ignored. According to Forrest and Wilkinson (1973), the yield stress is caused by the fact that it mainly depends on a mechanical locking of the fluid, which is essentially temperature independent. This is a possible explanation of the weak temperature dependency of the yields stress. Nevertheless, for higher temperature, τ_s may be sensitive to temperature.

The boundary conditions for U, V, and θ are as follows:

$$U(\eta, Z=0)=U_{cd};\ \theta(\eta, Z=0)=\theta_e \tag{6a}$$

The fully developed axial velocity and the inlet temperature are U_{cd} and θ_e, respectively.

$$\frac{\partial U}{\partial\eta}(\eta=0, Z)=\frac{\partial\theta}{\partial\eta}(\eta=0, Z)=V(\eta=0, Z)=0 \tag{6b}$$

$$U(Y=0, Z)=V(Y=0, Z)=0;\quad \frac{\partial\theta}{\partial Y}(Y=0, Z)=-\frac{\phi_p}{\bar{\lambda}\rho U_d^3}\quad\text{or}\quad \theta(Y=0, Z)=\theta_p \tag{6c}$$

Where ϕ_p and θ_p are, respectively, the wall heat density flux and the dimensionless wall temperature.

The established axial velocity profile U_{cd} is given by the following relation:

$$U_{cd}=\frac{1-\left[\dfrac{\eta}{\eta_0}-ap\right]^{m+1}}{\omega}\quad\text{if}\quad ap\le\frac{\eta}{\eta_0}\le 1$$

and

$$U_{cd}=\frac{1}{\omega}\quad\text{if}\quad 0\le\frac{\eta}{\eta_0}\le ap$$

where $ap=\eta_s/\eta_0=R_s/R$; R_s is the outer radius of the plug core.

and

$$\omega=1-2\left[\frac{(1-ap)^2}{m+3}+\frac{ap(1-ap)}{m+2}\right];\quad m=1/n$$

The relative dimension of the plug core ap can be calculated from the following relation:

$$ap=\frac{\tau_s}{\tau_p}\quad\text{with}\quad \tau_p=\tau_s+K\left(\frac{\mathrm{d}U_{cd}}{\mathrm{d}r}\right)_{r=R}^n$$

After some manipulations, ap is, thus, the solution of the following equation:

$$\frac{(1-ap)^{n+1}}{ap}=\frac{K(U_d/R)^n}{\tau_s\omega^n}(m+1)^n$$

Numerical solution

For the purpose of computation, it is not necessary to distinguish a state of shear ($\dot{\gamma}>0$) and a state of absolute rigidity ($\dot{\gamma}=0$). It is assumed that at very low shear rates, the fluid behaves as a Newtonian fluid with a very high viscosity, and that above a critical shear rate ($\dot{\gamma}_c$) a transition in behavior occurs; namely, yielding. After yielding, the fluid takes an apparent viscosity μ_a defined by the following:

$$\mu_a=\tau_s\left|\frac{\partial u}{\partial r}\right|^{-1}+K\left|\frac{\partial u}{\partial r}\right|^{n-1}$$

This biviscosity model is a convenient method of modeling materials with yield stress, which was adopted by several authors (O'Donovan and Tanner 1984). The analysis showed that for $(\partial u/\partial r)\le 10^{-3}\,\mathrm{s}^{-1}$, the results are quite insensitive to the cut-off value. In the present work, a value of $(\partial u/\partial r)_c=10^{-5}\,\mathrm{s}^{-1}$ is used.

Equations 1–5, as well as the associated boundary conditions, were solved by means of an extension of the linearized implicit finite difference of Bodoia and Osterle (1960). The axial convective term is approximated by the upstream difference and the radial convective and diffusional terms by the central difference. The integral representation of the continuity equation is determined by the trapezoidal rule of numerical integration. After some modifications, the finite difference equations form a tridiagonal matrix equation that can be solved efficiently by the Thomas algorithm.

Results and discussion

To discern the effect of the non-Newtonian behavior from that attributable to the temperature-dependent consistency on pressure drop and heat transfer, a numerical study in the case of constant physical properties is performed.

Temperature-independent consistency K

Assuming constant physical properties, the analysis of the thermal convection for a Herschel–Bulkley fluid enables us to determine the correction factor $Nu_{n,ap}/Nu_{New}$, that incorporates the modification of the wall shear rate by the rheological properties. For power-law fluids, Mizushina et al. (1967) have suggested to take the non-Newtonian behavior into consideration on the heat transfer by multiplying the Newtonian Nusselt number by $\Delta^{1/3}$, where Δ is the ratio of the wall shear rate compared to that which would have been obtained for a Newtonian fluid at the same flow rate. Joshi and Bergles (1980a) have confirmed this non-Newtonian correction for both entrance and fully developed regions, with a maximum deviation of 2% obtained for $n = 0.25$. This has led us to examine, for the Herschel–Bulkley fluids, the possibility of a correction by $\Delta^{*1/3}$, where Δ^* has the same meaning as Δ, and is given by the following:

$$\Delta^* = \frac{1}{4\omega}\frac{m+1}{1-ap_e}; \quad Nu_{n,ap} = \Delta^{*1/3}\cdot Nu_{New} \tag{7}$$

where Nu_{New} is the Newtonian Nusselt number.

We have observed for $n < 0.25$, and $ap_e > 0.7$ deviations between the Nusselt number calculated from Equation 7 and that evaluated numerically. For example, for $n = 0.25$, and $ap_e = 0.8$, a deviation of 16% is obtained at $X^+ = 10^{-2}$. A correction can be anticipated by using the asymptotic Nusselt number Nu_∞ (the expression of Nu_∞ is too long and is given in the Appendix). $Nu/Nu_{New} = Nu_\infty/4.36$. However, this time, deviations appear for the low values of X^+. A systematic study was performed for n ranging from 0.1 to 1 and ap_e from 0 to 0.9. It indicates that the non-Newtonian correction $\Delta^{*1/3}$ or Nu_x can be used in the entire duct, if n ranges from 0.3 to 1, and ap_e is less than 0.7. This conclusion is valid in the case of constant wall temperature as well as constant wall heat flux. The pressure drop can be characterized by the pressure gradient obtained in isothermal situation and for a fully developed axial velocity profile: $(-dp/dz)_{iso} = 2\tau_s/ap_eR$.

Temperature-dependent consistency K

Constant flux heating.

Axial velocity profile. It is well known that along a heated wall and under the effect of the decrease of the consistency K close to this wall, the wall shear rate increases, and the centerline velocity decreases because of the flow conservation. The relative radius of the plug core increases until it nearly fills up the whole section of the pipe. The asymptotic profile of axial velocity is almost flat and the reduced axial centerline velocity is then close to 1.

As an example, Figure 2 gives the evolution of the axial velocity profiles along the heating zone for $ap_e = 0.38$; $n = 0.5$; $b\phi_p D/2\lambda = 15$ and for various axial positions. The axial velocity profiles intersect at the same point M until the axial position where the plug core reaches this point. Beyond this point, this property is no longer confirmed. On the contrary, for Ostwald fluids, the velocity profiles intersect at the same point on the whole length of the heating zone, as shown in Figure 3. This intersection point separates the zone where there is an increase of the axial velocity from the zone where there is a decrease of the velocity.

A more convenient way to characterize the modifications of the axial velocity profile is to represent the evolution of the reduced axial centerline velocity $U_{max} = U(\eta = 0, Z)$ along the heating zone. As an example, Figure 4 shows, in semilogarithmic coordinates, the evolution of U_{max} as a function of the Cameron number X^+, for $n = 0.5$; $b\phi_p D/2\lambda$, denoted by $\beta = 15$ and for eight values of the relative size of the plug core ap_e going from 0 to 0.69. The "irregularities" observed at the establishing of the dynamic regime correspond to the axial position where the plug core reaches the intersection point of the axial velocity profiles. We can note a discontinuity for U_{max}, when ap_e tends toward zero.

In opposition to the Forest and Wilkinson indication (1973), it is possible to determine a pseudodynamic entrance length Xe^+ as the distance from the inlet section, for which the centerline velocity is equal to 1.01 of the limiting value. Figure 5 shows the evolution of the pseudodynamic

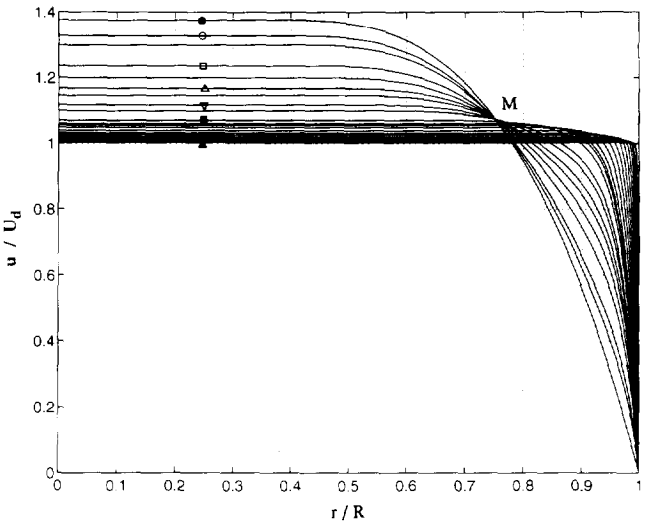

Figure 2 Evolution of the axial velocity profile along the heating zone, case of constant flux heating: $n = 0,5$; $ap_e = 0,38$; $\beta = 15$ (● is $X^+ = 0$; ○ is $X^+ = 4.5\,10^{-5}$; □ is $X^+ = 2.7\,10^{-4}$; △ is $X^+ = 6.7\,10^{-4}$; ▽ is $X^+ = 1.3\,10^{-3}$; ■ is $X^+ = 2.7\,10^{-3}$; and ▲ is $X^+ = 9.8\,10^{-2}$)

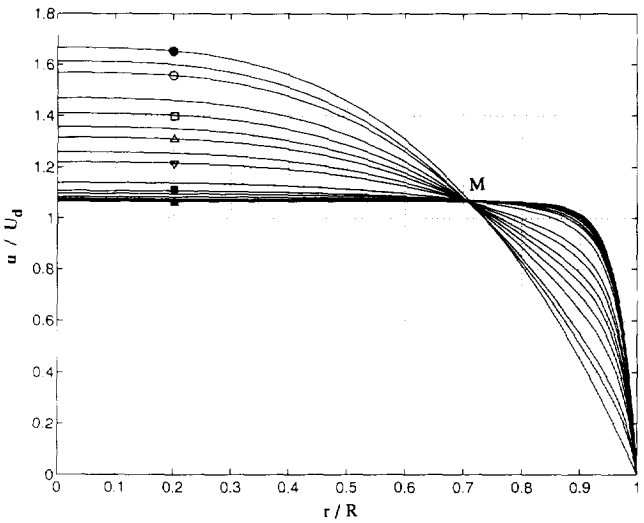

Figure 3 Evolution of the axial velocity profile along the heating zone, case of constant flux heating: $n = 0,5$; $ap_e = 0$; $\beta = 15$ (● is $X^+ = 0$; ○ is $X^+ = 4.5\,10^{-5}$; □ is $X^+ = 2.7\,10^{-4}$; △ is $X^+ = 6.7\,10^{-4}$; ▽ is $X^+ = 1.3\,10^{-3}$; ■ is $X^+ = 2.7\,10^{-3}$; and ▲ is $X^+ = 9.8\,10^{-2}$)

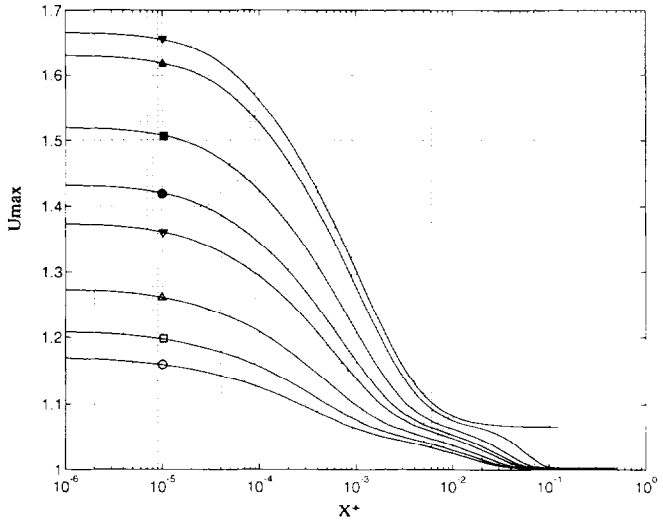

Figure 4 Evolution of U_{max} along the heating zone, case of constant flux heating: $n = 0.5$ and $\beta = 15$ (▼ is $ap_e = 0$; ▲ is $ap_e = 0.04$; ■ is $ap_e = 0.18$; ● is $ap_e = 0.29$; ∇ is $ap_e = 0.38$; ▽ is $ap_e = 0.52$; △ is $ap_e = 0.62$; and ○ is $ap_e = 0.69$)

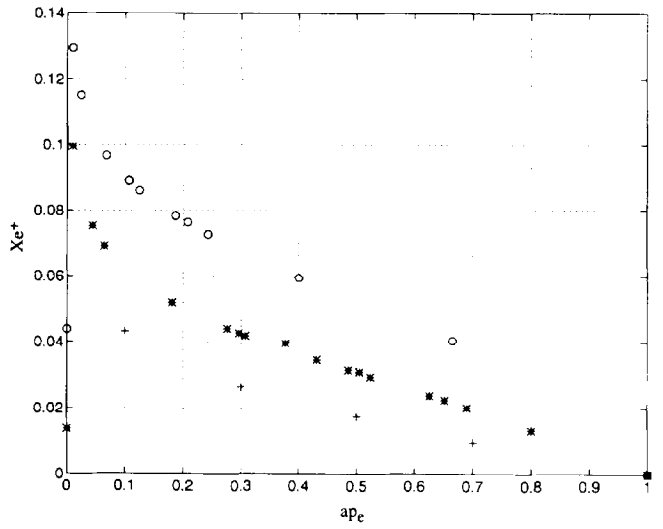

Figure 5 Pseudodynamic entrance length Xe^+ *versus* the dimension of the plug core ap_e, case of constant flux heating: $\beta = 15$ (○ is $n = 1$; * is $n = 0.5$; and + is $n = 0.25$)

entrance length Xe^+ for $\beta = 15$ and for three values of the power-law index $n = 1$, 0.5 and 0.25. The numerical results show that: (1) X_e^+ decreases when ap_e increases and tends toward zero when ap_e tends toward 1; (2) a discontinuity appears at the abscissa point $ap_e = 0$, as Xe^+ seems to increase when ap_e tends towards zero; whereas, for $ap_e = 0$, the value of Xe^+ exists and is equal to 0.013; (3) when the power-law index decreases, the fluidification becomes more important, and development of the dynamic field approaches very fast; (4) as for the effect of the dimensionless grouping β is concerned, it favors the developemnt of the thermal and dynamic fields. Once more, for a yield stress fluid X_e^+ increases when β tends toward zero.

Pressure drop. In an isothermal situation, the pressure gradient $(dp/dz)_{iso}$ is given by: $(-dp/dz)_{iso} = 2\tau_s/(ap_eR)$. In the presence of heating and in order to underline the effect of the thermodependency, it is agreed to consider a ratio of (dp/dz) to the gradient of isothermal pressure. This ratio is also equal to the ratio Cf^* of the friction coefficient to the isothermal one. As formerly, Cf^* depends on n, ap_e, β, and X^+. In Figure 6, $-\log Cf^*$ is plotted against Cameron number X^+ for eight values of the relative radius of the plug core ap_e. Because the viscosity is decreasing with temperature, Cf^* is lower than 1. Moreover, for each curve, three parts can be distinguished in the evolution of Cf^* *versus* X^+. Firstly, a low evolution with X^+, close to the inlet section because of the progressive increase of the wall temperature, then an exponential decrease of Cf^*, and last, a nearly constant value corresponding to the development of the dynamic field. When the dynamic regime is established, $-dp/dz$ is equal to $2\tau_s/R$, and $Cf^* = ap_e$. Figure 6 also shows that the more the plug core dimension is important, the less the thermodependence effect is marked. The effect of β, of course, contributes to a decrease of the pressure drop. The power-law index has practically no effect when it varies between 0.5 and 1.

It is useful to present the results as correlations. In the thermal entrance region, a simple idea consists in writing that Cf^* is equal to what would be obtained for an Ostwald fluid when $ap_e = 0$ and is equal to 1 when $ap_e = 1$. If we anticipate a linear evolution as a function of ap_e between these two limits, we will be able to write the following:

$$Cf^*_{(ap_e \neq 0)} = Cf^*_{(ap_e = 0)}[1 - ap_e] + ap_e$$

with (8)

$$Cf^*_{(ap_e = 0)} = \exp[-2{,}5\beta(X^+)^{-0.64}]$$

However, we can observe that the relation (8) can also be applied to large values of X^+, where the dynamic field becomes developed, and $Cf^* = ap_e$. Last, we have checked that the maximal deviation between the values given by the correlation (8) and the numerical results is of 5% for $0 \leq ap_e \leq 0.7$; $0.3 \leq n \leq 1$ and $3.75 \leq \beta \leq 37.5$.

The relation (8) gives also the evolution of $ap(X^+)$, because $Cf^* = ap_e/ap(X^+)$. If we consider the position of X^+ measured

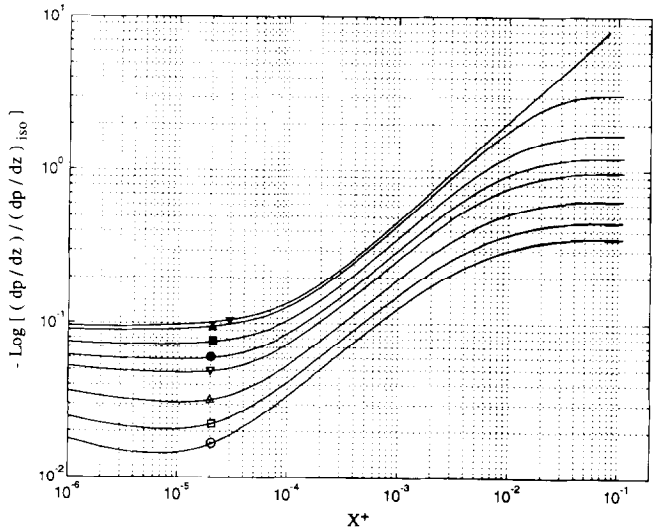

Figure 6 Evolution of the reduced pressure gradient along the heating zone, case of constant flux heating: $n = 0.5$; $\beta = 15$ (▼ is $ap_e = 0$; ▲ is $ap_e = 0.04$; ■ is $ap_e = 0.18$; ● is $ap_e = 0.29$; ▽ is $ap_e = 0.38$; △ is $ap_e = 0.52$; □ is $ap_e = 0.62$; and ○ is $ap_e = 0.69$)

from the inlet section for which, for example $ap(X^+) = 0.9$, we find:

$$X^+ = \left[-\frac{1}{2.5\beta} \log \frac{ap_e}{9(1 - ap_e)} \right]^{1/0.64}$$

This expression indicates that the establishment length of the dynamic regime tends toward the infinity when ap_e or β tend toward zero, as mentioned in the previous paragraph.

Heat transfer. The flow structure depends upon the size of the plug core, on the power-law index, and on the dimensionless grouping β. Therefore, it is the same for the exchange rate. Figure 7 illustrates the development of the temperature profile along the pipe for $\beta = 15$, $n = 0.5$, and $ap_e = 0.38$. The evolution of the thermal boundary layer $\delta(X^+)$ and of $ap(X^+)$ have also been represented. The axial position where the thermal boundary layers meets the plug core has been identified. The corresponding axial velocity profile has been brought to this position. The thickness $\delta(X^+)$ is defined as the distance from the wall for which $\theta_p - \theta(\delta) = 0.99(\theta_p - \theta_e)$.

As far as the heat transfer rate is concerned, Figure 8 gives the evolution of the Nusselt number against the Cameron number for $\beta = 15$, $n = 0.5$, and $ap_e = 0.38$ and for six values of β: 3.75; 7.5; 11.25; 15; 22.5; and 37.5. Three areas can be distinguished. In the first area, the Nusselt number decreases from the inlet section onward because of the increase of the thickness of the thermal boundary layer. The second area is an area of transition, where for some values of ap_e and β (see the curve relative to $\beta = 3.75$), the Nusselt number decreases until it reaches a minimum. It then increases because of the increase of the wall shear rate. The third area corresponds to the development of the thermal regime where the Nusselt number tends asymptotically toward a limiting value equal to 8. This latter value is related to the fact that the asymptotic velocity profile is flat. In the nonthermodependent case, the asymptotic Nusselt number Nu_∞ depends upon ap_e. In Figure 8 also, the classical result relative to the increase of the Nusselt number with the dimensionless grouping β can be found. The effect of ap_e is characterized, on the one hand, by a modification of the axial velocity profile, and on the other hand, by a decrease of the effects of thermodependency. The more ap_e is important, the less the thermodependency effect is significant.

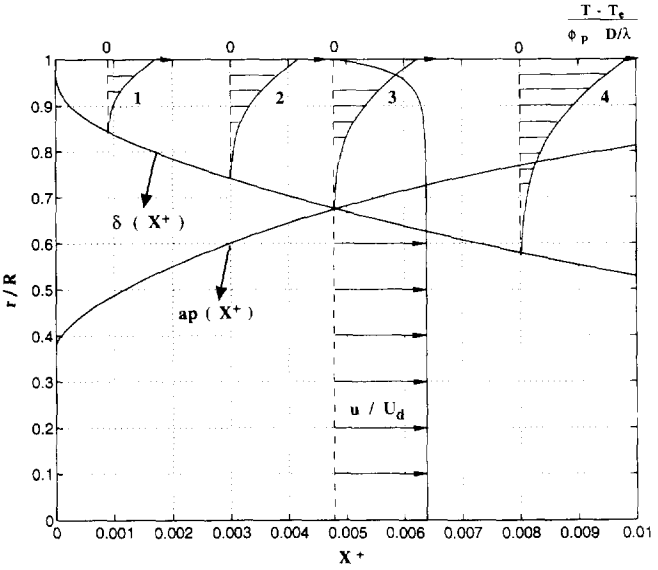

Figure 7 Structure of the thermal field, case of constant flux heating: $n = 0.5$; $ap_e = 0.38$; $\beta = 15$ (1) $X^+ = 0.9\ 10^{-3}$; (2) $X^+ = 3\ 10^{-3}$; (3) $X^+ = 4.8\ 10^{-3}$; and (4) $X^+ = 8\ 10^{-3}$

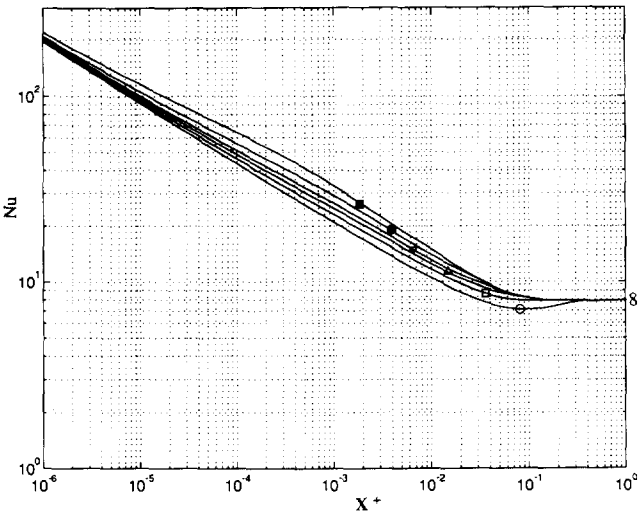

Figure 8a Evolution of the local Nusselt number along the heating zone, case of constant flux heating: $n = 0.5$; $ap_e = 0.38$ (○ is $\beta = 3.75$; □ is $\beta = 7.50$; △ is $\beta = 11.25$; ▽ is $\beta = 15.0$; ● is $\beta = 22.50$; and ■ is $\beta = 37.50$)

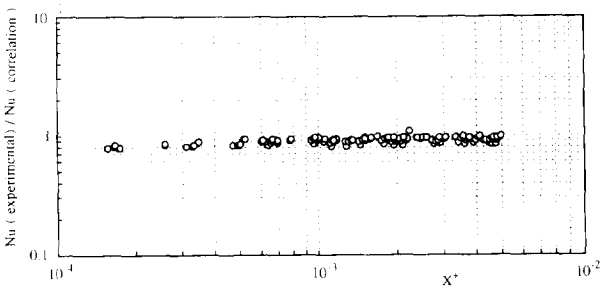

Figure 8b Comparison of the numerical results with the experimental data

If we take as a basis an extension of Lévêque method for the yield stress fluids, it is possible to write in the thermal entrance zone $Nu \sim \Phi_p^{1/3} X^{+(-1/3)}$ ($\sim$ means proportional); Φ_p is a dimensionless wall shear rate. Combining non-Newtonian and consistency variation corrections, we can write:

$$\Phi_p = \Phi_{p,rp} = \frac{\Phi_{p,cp}}{\Phi_{p,\mathrm{New}}} \cdot \frac{\Phi_{p,rp}}{\Phi_{p,cp}} \cdot \Phi_{p,\mathrm{New}} = \Delta^* \cdot \Delta' \cdot \Phi_{p,\mathrm{New}}$$

The ratio of the nonisothermal to isothermal wall velocity gradient of the yield stress fluid is Δ'. It accounts for the modification of the wall shear rate with the variation of the consistency K with temperature.

In the thermal entrance zone, the Nusselt number can be written as follows:

$$Nu = 1.64 \left[\frac{X^+}{\Delta^* \Delta'} \right]^{-1/3}$$

with

$$\Delta'^{1/3} = \beta^{\alpha}$$

and

$$\alpha = (0.13 - 0.085\, n) \cdot (1 - ap_e) \cdot [2.3 - 1.3(1 - ap_e)]$$

In setting up a correlation, we take care to introduce dimensionless groupings to make their use more convenient. Thus, in the former equation, the grouping $b\phi_p D/2\lambda$ intervenes rather than the ratio of the consistencies K_m/K_p. The expression of Δ' shows once more that the effects of thermodependency decrease in the presence of a yield stress. This result has been qualitatively mentioned by Naïmi et al. (1990).

When the thermal field is established, the Nusselt number is practically equal to 8. Following Churchill and Usagi method (1972), a unique correlation on the whole length of the pipe is searched as follows:

$$\mathrm{Nu} = 8\left[1 + \left(0.205\left(\frac{X^+}{\Delta'\Delta^*}\right)^{-1.3}\right)^{\xi}\right]^{1/\xi}$$

The optimal value of ξ is the one that enables us to approach the numerical results as close as possible. We find $\xi = 3$. Last, the former equation can be written as follows:

$$\mathrm{Nu} = 8\left[1 + 8.61.10^{-3}\frac{\Delta'\Delta^*}{X^+}\right]^{1/3} \tag{9}$$

for $0.02 \leq ap_e \leq 0.7$; $0.3 \leq n \leq 1.0$, and $3.75 \leq \beta \leq 37.5$.

The maximum deviation of the heat transfer coefficient calculated from Equation 9 and the numerical results is 15%. This maximum is obtained at $X^+ = 10^{-5}$ and at $X^+ = 5\,10^{-3}$. Figure 8b shows a comparison between the numerical correlation and experimental results of Nouar et al. (1994). For the majority of the points, the difference is less than 15%.

Heating at constant wall temperature.

Axial velocity profile. Far downstream, the temperature becomes uniform across the tube at a value approaching T_p, and the axial velocity profile is then fully developed. If the fluid had had no yield stress, the velocity profile would have reverted back to its isothermal value when the temperature became uniform across the tube. However, the existence of a yield stress and the change in the wall shear stress changes the dimension of the plug core, so the asymptotic axial velocity profile is not the same as that at the inlet to the heated section.

The redistribution of the flow takes place in two stages.

(1) In the first stage, the wall shear rate increases, and the centerline velocity decreases. Nevertheless, the shape of the axial velocity profiles is different from that observed in the case of a constant flux heating. A high increase of the wall shear rate occurs, because the tube wall is subjected to a sudden increase in temperature at the start of the heated section.

(2) In the second stage, the axial velocity profile that is flattened tends toward a developed profile. This second stage is characterized by a decrease of the wall shear rate and an increase of the centerline velocity.

As with constant flux heating, it is more convenient to represent the evolution of the axial velocity profiles through the evolution of U_{max} along the heating zone. The dimensionless parameters that rule the problem are: the power-law index n; the dimensionless number, $\beta' = b(T_p - T_e)$; and, of course, the relative width of the plug core ap_e at the inlet of the heating zone. In Figure 9, the evolution of U_{max} has been represented according to X^+ for $n = 0.5$; $\beta' = 1$, and for various values of the size of the plug core. The minimum of each curve corresponds to the higher limit of the first stage in the redistribution of the flow. In this case, it is possible to define another pseudodynamic entrance length Xe_1^+, representing the extension of the first stage. If we analyze the effect of the various parameters n, ap_e, and β on Xe_1^+, we observe that: (1) the extension of the first stage is as consequent as ap_e is low, when $ap_e = 0$, no discontinuity is observed; (2) a decrease of the power-law index leads to a smaller extension of the first stage; and (3) the more the dimensionless number β is large, the more Xe_1^+ is low. In the second stage, the higher ap_e is, the lower the evolution of U_{max} following X^+ is

Pressure drop. As previously, we consider the evolution of the ratio (dp/dz) on $(dp/dz)_{iso}$ written as Cf^* along the heated section, which depends upon n, ap_e, and β. In Figure 10, $-\log Cf^*$ is plotted against the Cameron number X^+ for eight values of the relative width of the plug core ap_e going from 0 to 0.69. As with constant flux heating, the increase of ap_e cuts down the effects of thermodependency. As for the effect of β,

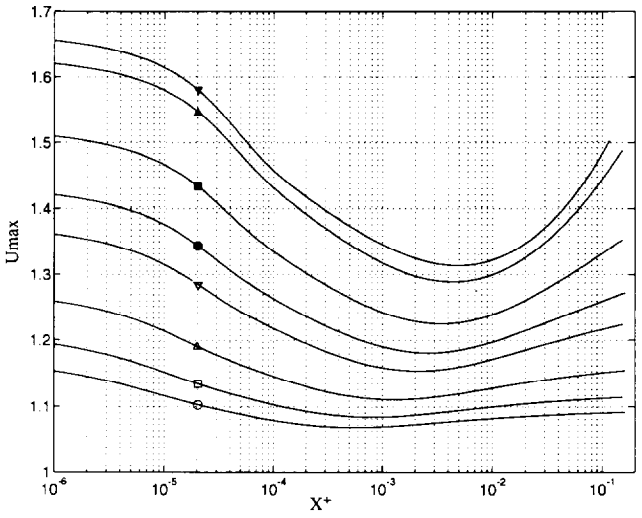

Figure 9 Evolution of U_{max} along the heating zone, case of constant wall temperature heating: $n = 0.5$, and $\beta' = 1$ (▼ is $ap_e = 0$; ▲ is $ap_e = 0.04$; ■ is $ap_e = 0.18$; ● is $ap_e = 0.29$; ▽ is $ap_e = 0.38$; △ is $ap_e = 0.52$; □ is $ap_e = 0.62$; and ○ is $ap_e = 0.69$)

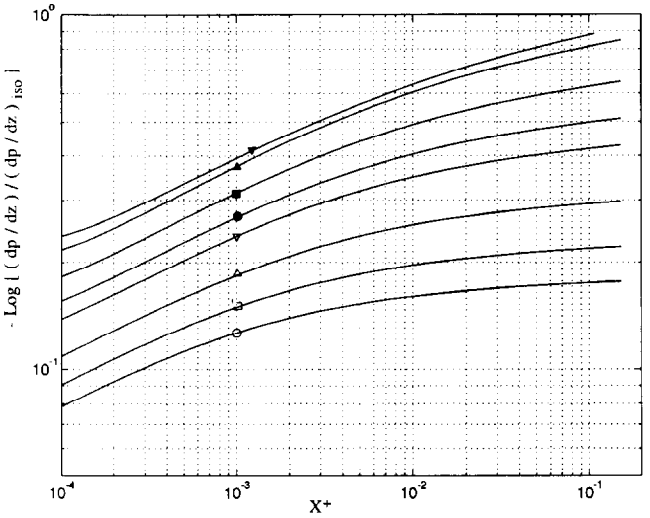

Figure 10 Evolution of the reduced pressure gradient along the heating zone, case of constant wall temperature heating: $n = 0.5$; $\beta' = 1$ (▼ is $ap_e = 0$; ▲ is $ap_e = 0.04$; ■ is $ap_e = 0.18$; ● is $ap_e = 0.29$; ▽ is $ap_e = 0.38$; △ is $ap_e = 0.52$; □ is $ap_e = 0.62$; and ○ is $ap_e = 0.69$)

it is clear that Cf^* decreases when β increases because of the decrease of the viscosity.

It is always interesting to have a correlation that allows the calculation of the pressure drop according to the various parameters that govern the problem. To use the Churchill and Usagi (1972) method, the asymptotic behavior has been searched for close to the inlet and further downstream. The inlet area corresponds to the first stage in the redistribution of the flow: $Cf_e^* = \exp(-\Psi)$, with $\Psi = (1 - ap_e)\cdot(0.42n^2 - 0.07n + 1.97)\cdot\beta'\cdot X^{+0.17+0.13n}$. When the dynamic condition is developed, $Cf^* = Cf_x^*$ and is given by the following:

$$Cf_x^* = \frac{ap_e}{ap_x} \quad \text{if} \quad ap_e \neq 0; \quad Cf_x^* = \exp[-b(T_p - T_e)]$$

$$\text{if} \quad ap_e = 0$$

The application of Churchill and Usagi (1972) method leads to an expression of Cf^* as follows:

$$Cf^* = [(Cf_x^*)^8 + (Cf_x^*)^8]^{1.8}; \quad 0.3 \leq n \leq 1; \quad 0 \leq ap_e \leq 0.7$$

and $\quad 0.5 \leq \beta' \leq 2X^+ \geq 10^{-4}$

This expression has been confirmed in the different ranges of variation of the various dimensionless parameters mentioned below with a maximal deviation of 10% when compared to the numerical results.

Heat transfer. The structure of the thermal field can be illustrated by Figure 11, where some temperature profiles have been drawn as well as the evolution of the thermal boundary layer and the width of the plug core. The evolution of the Nusselt number along the heating zone for $n = 0.5$ $ap_e = 0.38$ for four values of β': 0.5; 1; 1.5 and 2 is given in Figure 12. Again, we notice an increase of the Nusselt number attributable to the thermodependency. The variation of ap by the rheological properties modifies the wall shear rate and, therefore, the heat transfer ratio. This modification is integrated in the nonthermodependent case by the correction factor $\Delta^{*1/3}$.

Last, a unique correlation has been sought for the entire

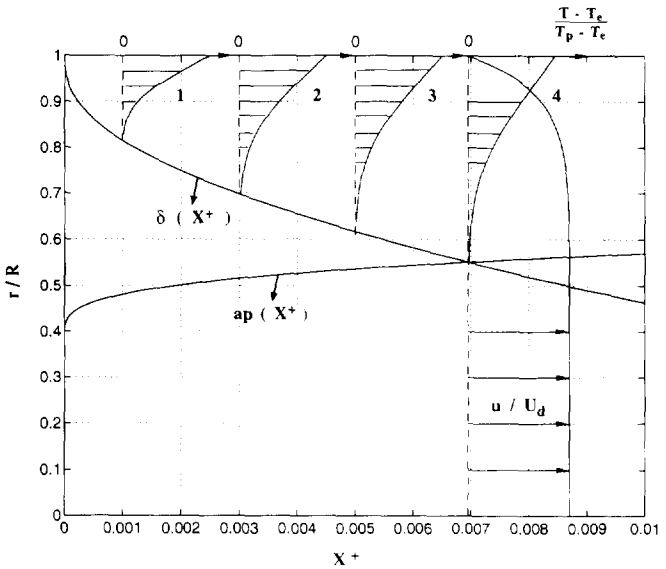

Figure 11 An example of the structure of the thermal field, case of constant wall temperature heating: $n = 0.5$; $\beta' = 1.$; $ap_e = 0.38$ (1) $X^+ = 10^{-3}$; (2) $X^+ = 3\ 10^{-3}$; (3) $X^+ = 5.\ 10^{-3}$; and (4) $X^+ = 6.9\ 10^{-3}$

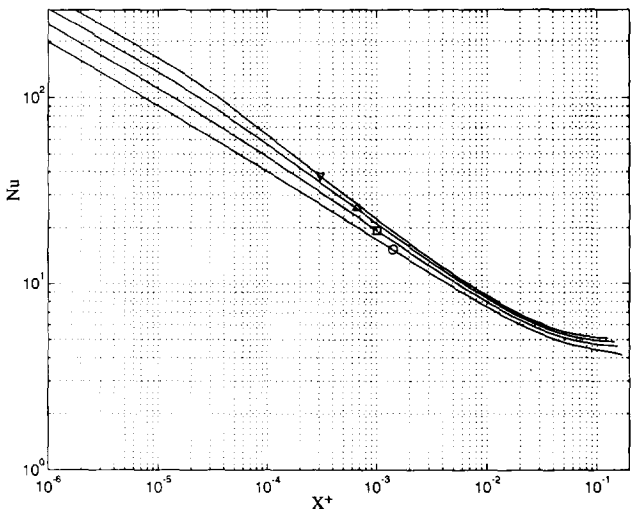

Figure 12 Evolution of the Nusselt number along the heating zone, case of constant wall temperature heating: $n = 0.5$; $ap_e = 0.38$ (○ is $\beta' = 0.5$; □ is $\beta' = 1$; △ is $\beta' = 1.5$; and ▽ is $\beta' = 2$)

length of the pipe according to Churchill and Usagi (1972) method:

$$\mathrm{Nu} = \mathrm{Nu}_x\left[1 + \left(\frac{1{,}35}{\mathrm{Nu}_x}\left(\frac{X^-}{\Delta^*\Delta'}\right)^{-1/3}\right)^6\right]^{1/6}$$

with $\Delta'^{1/3} = \exp(0.1/n)[(0.9 - 0.09n) + (0.13 + 0.08n\beta')]\cdot f(ap_e)$, and $f(ap_e) = 1 - 0.02ap_e - 0.1ap_e^2$; if $ap_e \leq 0.7$; $n \geq 0.3$, and in the case of nonviscous dissipation, the asymptotic Nusselt number is $\mathrm{Nu}_x = (\mathrm{Nu}_{\mathrm{New}})_x(\Delta^{*1/3})_x = 3.66(\Delta^{*1/3})_x$.

The maximum deviation between the Nusselt number calculated from correlation (10), and the numerical results is 20%. The heat transfer with constant wall temperature is more difficult to correlate than the case of constant wall heat flux because of a sudden increase of temperature in the entrance section.

At $X^+ = 0.1$, the variation of Nusselt number *versus* the Cameron number does not present an asymptotic behavior. It is particularly visible on the curve corresponding to $\beta' = 0.5$ ($Tp - T_e$). As a matter of fact, far downstream, the conventional local Nusselt number continues to decrease, and for a certain axial position, it becomes infinite with negative value. Further downstream, the local Nusselt number attains an asymptotic value that is higher than that for $\mathrm{Br} = 0$. This evolution is because of the viscous dissipation. According to Lawal and Mujumdar (1992), the fluid temperature rises because of heat transfer from the wall and viscous heating. This latter mechanism of heating depends upon the shear rate, which is highest in the wall region. Hence; while T_p is still greater than T_m, an axial location is reached where the thermal gradient becomes zero, so that the Nusselt number also becomes zero. Thereafter, there is a heat flux reversal, with the fluid heating the wall. The bulk temperature continues to rise until a location is reached where it becomes equal to the wall temperature. At this point, the local Nusselt number distribution exhibits a singularity.

In our study, the Brinkman number defined by $\mathrm{Br} = \mu_0 U_d^2/[\lambda(T_e - T_p)]$ varies between 0 and -0.01. For a constant wall heat density rate, the effect of viscous dissipation is not significant for the range of Brinkman numbers considered. For a constant wall temperature, the effect of viscous dissipation on the pressure gradient is weak. Concerning the Nusselt number, the effect appears at large values of X^+: $X^+ \geq 0.01$.

Conclusion

A numerical analysis of the thermal convection for a Herschel–Bulkley fluid in a cylindrical pipe has been performed. Two boundary conditions have been considered, constant wall heat flux and constant wall temperature. The equations of conservation have been approximated by a finite-difference method with a fully implicit scheme. All the physical properties of the fluid are assumed to be constant except for the consistency K, whose variation with the temperature is given by $K = K_0 \exp(-bT)$.

Constant wall flux heating

The thermal gradients at the wall induce a fluidification of the product. An increase of the wall shear rate balanced by a decrease of the velocity on the axis of the pipe is observed. The axial velocity profile evolves until it reaches an almost flat profile. This redistribution of the flow gives rise to a radial velocity directed from the center of the flow toward the heated wall. After analyzing the evolution of the flow structure in the entire heating zone, it has been possible to interpret the variation of the pressure gradient and of the heat transfer rate as a function of the rheological parameters and of the dimensionless grouping β. The following correlations relative to the pressure gradient and to the local Nusselt number depending upon various dimensionless parameters have been offered:

$$Cf^*_{(ap_e \neq 0)} = Cf^*_{(ap_e = 0)}[1 - ap_e] + ap_e$$

with

$$Cf^*_{(ap_e = 0)} = \exp[-2.5\beta(X^+)^{-0.64}]$$

for $0 \leq ap_e \leq 0.7$; $0.3 \leq n \leq 1$, *and* $3.75 \leq \beta \leq 37.5$, where

$$Cf^* = \frac{(dp/dz)_{cp}}{(dp/dz)_{cp}} \quad \text{and} \quad \beta = b\phi_p D/2\lambda$$

and

$$\mathrm{Nu} = 8\left[1 + 8.61.10^{-3}\frac{\Delta'\Delta^*}{X^+}\right]^{1.3}$$

for $0.02 \leq ap_e \leq 0.7$; $0.3 \leq n \leq 1.0$, and $3.75 \leq \beta \leq 37.5$ with $\Delta'^{1/3} = \beta^{\alpha}$; $\alpha = [0.13 - 0.085n] \cdot [1 - ap_e] \cdot [2.3 - 1.3(1 - ap_e)]$; $\Delta^* = (1/4\omega)(m + 1)/(1 - ap_e)$; $\omega = 1 - 2[(1 - ap_e)^2/(m + 3) + ap_e(1 - ap_e)/(m + 2)]$; $m = 1/n$.

Constant wall temperature heating

Because the asymptotic profile of temperature is flat $T(r) = T_p$, the redistribution of the flow takes place in two stages. In the first stage, the wall shear rate increases, and the centerline velocity decreases. At the end of the first stage, the axial velocity profile is flattened. In the second stage, the "flattened" profile tends asymptotically toward an established isothermal profile, calculated at the wall temperature. As with constant flux heating, the pressure gradient and the heat transfer ratio are analyzed according to the evolution of the flow structure. Finally, the following correlations are presented for the pressure gradient and the heat transfer rate.

$$Cf^* = [(Cf^*_\infty)^8 + (Cf^*_e)^8]^{1.8}; \quad 0.3 \leq n \leq 1; \; 0 \leq ap_e \leq 0.7$$

and $\quad 0.5 \leq \beta' \leq 2$

$$Cf^*_e = \exp(-\Psi)$$

with

$$\Psi = (1 - ap_e) \cdot (0.42n^2 - 0.07n + 1.97) \cdot \beta' \cdot X^{+0.17+0.13n};$$

$$Cf^*_\infty = \frac{ap_e}{ap_\infty} \quad \text{if} \quad ap_e \neq 0;$$

$$Cf^*_\infty = \exp[-b(T_p - T_e)] \quad \text{if} \quad ap_e = 0$$

and

$$\mathrm{Nu} = \mathrm{Nu}_\infty\left[1 + \left(\frac{1.35}{\mathrm{Nu}_\infty}\left(\frac{X^+}{\Delta^*\Delta'}\right)^{-1/3}\right)^6\right]^{1/6}$$

with

$$\Delta'^{1/3} = \exp(0.1/n)[(0.9 - 0.09n) + (0.13 + 0.08n\beta')] \cdot f(ap_e)$$

and

$$f(ap_e) = 1 - 0.02ap_e - 0.1ap_e^2$$

if $ap_e \leq 0.7$; $n \geq 0.3$, and without viscous dissipation, the asymptotic Nusselt number is $\mathrm{Nu}_\infty = (\mathrm{Nu}_{\mathrm{New}})_\infty(\Delta^{*1/3})_\infty = 3.66(\Delta^{*1/3})_\infty$.

Acknowledgments

This study has been financially supported by the Heat Transfer and Aerodynamics Department of the Research and Development Division (EDF).

References

Bodoia, J. R. and Osterle, J. F. 1960. Finite difference analysis of plane Poiseuille and Couette flow developments. *Appl. Sci. Res.*, Sec. A10, 265–276

Chandrupatla, A. B. and Sastri, V. M. K. 1978. Constant wall temperature entry length laminar flow and heat transfer to a non-Newtonian square duct. *Proc. 8th Int. Heat Transfer Conf.*, Toronto, **5**, 323–328

Churchill, S. W. and Usagi, R. 1972. A general expression for the correlation of rates of transfer and other phenomena. *J. Heat Transfer*, **98**, 1121–1122

Forrest, G. and Wilkinson, W. L. 1973. Laminar heat transfer to temperature-dependent Bingham fluids in tubes. *Int. J. Heat Mass Transfer*, **16**, 2377–2391

Hirai, E. 1959. Theoretical explanation of heat transfer in the laminar region of Bingham fluid, *AIChEJ.*, **5**, 130–133

Joshi, S. and Bergles, A. E. 1980a. Analytical study of heat transfer to laminar in tube flow of non-Newtonian fluids, *AIChE, Symp. Series*, **76**, 270–279

Joshi, S. and Bergles, A. E. 1980b. Experimental study of laminar heat transfer to in-tube flow of non-Newtonian fluids. *J. Heat Transfer*, **102**, 397–401

Kahine, K., Nguyen, V. T. and Lebouché, M. 1991. Ecoulement et transfert de chaleur pour des fluides rhéofluidifiants themodépendants, *Actes du 10ème Congrès Français de Mécanique*, Paris, **2**, 41–44

Kwant, P. B., Zwaneveld, A. and Dijkstra, F. C. 1973a. Non-isothermal laminar pipe flow—I. *Theoretical Chem. Eng.*, **28**, 1303–1316

Kwant, P. B., Fierens, R. H. E. and Van Der Lee, A. 1973b. Non-isothermal laminar pipe flow—II. Experimental, *Chem Eng.* **28**, 1317–1330

Lawal, A. and Mujumdar, A. S. 1992. The effects of viscous dissipation on heat transfer to power law fluids in arbitrary cross-sectional ducts. *Wärme-und Stoffübertragung*, **27**, 437–446

Lin, T. and Shah, V. L. 1978. Numerical solution of heat transfer to yield power law fluids flowing in the entrance region, *Proc. 6th Int. Heat Transfer Conf.*, Toronoto, **5**, 317–322

Lyche, B. C. and Bird, R. B. 1956. The Graetz–Nusselt problem for a power-law non-Newtonian fluid. *Chem. Eng. Sci.*, **6**, 35–91

Metzner, A. B., Vaughn, R. D. and Houghton, V. M. 1957. Heat transfer to non-Newtonian fluids. *AChE J.*, **3**, 92–100

Mizushina, T., Ito, R., Kuriwake, Y. and Yahikazawa, K. 1967. Boundary-layer heat transfer in a circular tube to Newtonian and non-Newtonian fluids. *Kagaku-Kogaku*, **31**, 250–255

Naïmi, M., Devienne, R. and Lebouché, M. 1990. Etude dynamique et thermique de l'écoulement de Couette Taylor–Poiseuille: Cas d'un liquide présentant un seuil d'écoulement. *Int. J. Heat Mass Transfer*, **33**, 381–391

Nouar, C., Devienne, R. and Lebouché, M. 1994. Convection thermique pour un fluide de Hershel–Bulkley dans la région d'entrée d'une conduite. *Int. J. Heat Mass Transfer*, **37**, 1–12

O'Donovan, E. V. and Tanner, R. I. 1984. Numerical study of the Bingham squeeze film problem. *J. Non-Newtonian Fluid Mech.*, **15**, 75–83

Pigford, R. L. 1955. Non-isothermal flow and heat transfer inside vertical tubes. *Chem. Eng. Prog. Symp.*, Series 17, 79–92

Scirocco, V., Devienne, R. and Lebouché, M. 1985. Ecoulement laminaire et transfert de chaleur dans la zone d'entrée d'un tube. *Int. J. Heat Mass Transfer*, **28**, 91–99

Vradis, C. G., Dougher, J. and Kumar, S. 1992. Entrance pipe flow and heat transfer for a Bingham plastic. *Int. J. Heat Mass Transfer*, **36**, 543–552

Whiteman, I. R. and Drake, W. E. 1958. Heat transfer to flow in around tube with arbitrary velocity distribution. *Trans. ASME*, **80**, 728–732

Wissler, E. H. and Schechter, S. C. 1959. The Graetz–Nusselt problem (with extension) for a Bingham plastic. *Chem. Eng. Prog. Symp. Ser.*, **55**, 203

Appendix

The asymptotic Nusselt number in the case of independent physical properties and under the boundary condition of constant wall heat density flux is as follows:

$$\mathrm{Nu}_r = \frac{2\omega^2}{0.25 + 4G(1 - ap_e)^{-2m-2}}$$

$$G = \frac{(1 - ap_e)^{2m+5}(m + 4 + ap_e)}{(m + 2)(m + 3)(m + 4)(m + 5)} + \frac{(1 - ap_e)^{2m+5}(2m + 5 + ap_e)}{2(m + 2)^2(m + 3)(2m + 5)} + \frac{(1 - ap_e)^{2m+6}}{(m + 2)^2(m + 3)^2} - \frac{(1 - ap_e)^{2m+4}(m^2 + 2ap_e m + 7m + 2ap_e^2 + 6ap_e + 12)}{(m + 2)(m + 3)(m + 4)(m + 5)} + \frac{1}{(m + 2)^2(m + 3)^2} \sum_{l=0}^{2m+5} C_{2m+6}^{l}[(-ap_e)^l(1 - ap_e^{2m+6-l})] + \frac{ap_e^{2m+6}}{(m + 2)^2(m + 3)^2} \log ap_e$$